Supporting Information

Structurally-selective geminate rebinding dynamics of solvent-caged radicals studied with non-equilibrium infrared echo spectroscopy

Carlos R. Baiz, Robert McCanne and Kevin J. Kubarych*

Email: kubarych@umich.edu

Department of Chemistry, University of Michigan
930 N. University Ave, Ann Arbor, MI 40109

Temperature-Dependent Infrared Absorption Spectra

Temperature-dependent absorption spectra were collected using a standard Fourier-transform infrared spectrometer. The sample solution was flowed using a flow-cell equipped with a 100μm spacer. While flowing continuously, the solution was slowly cooled by placing the reservoir in an acetone/dry-ice bath and FTIR spectra were recorded between -7 and 27 ^{o}C. The equilibrium constant was obtained by monitoring the ratio of the center peak at 1958 cm^{-1} (*trans* + *gauche*), to the high frequency 2013 cm^{-1} (*gauche* only). Since the two isomers have overlapping transitions, *ab-initio* derived molar absorptivities were used for calculating the equilibrium constants from the measured FTIR spectra. A van 't Hoff plot (Figure S.1) reveals a $\Delta H = 3.16 \pm 0.94$ kJ mol^{-1} and $\Delta S = -24.5 \pm 3.7$ J mol^{-1} K^{-1}.

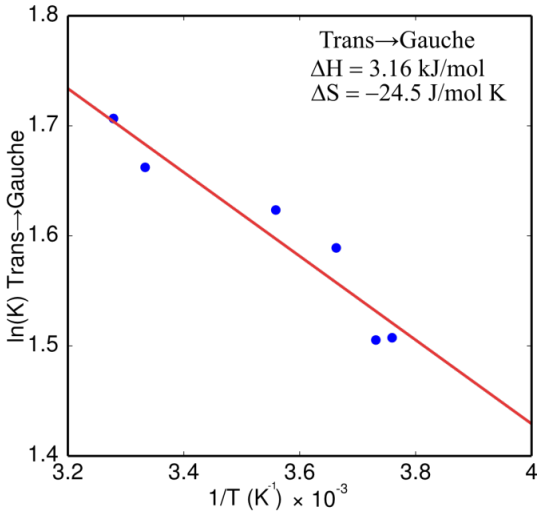

Figure S.1 – Plot of 1/T versus ln(K) for *Trans*→*Gauche* isomerization reaction of $[CpMo(CO)_3]_2$ in ethyl acetate.

Description of Experimental Setup

Equilibrium and transient Fourier-transform two-dimensional infrared spectra of $[CpMo(CO)_3]_2$ were measured using an optical setup described previously.[1-2] In brief, three (~100 fs FWHM) mid-infrared pulses with wave vectors $\mathbf{k}_1$ $\mathbf{k}_2$ and $\mathbf{k}_3$ were applied to the sample and the emitted signal field was measured in the $\mathbf{k}_s = -\mathbf{k}_1+\mathbf{k}_2+\mathbf{k}_3$ direction by interferometric superposition with a phase-stable reference pulse. The signal was upconverted into the visible in slightly wedged 5% MgO doped $LiNbO_3$ crystals using a highly-chirped pulse centered at 800 nm, and detected using a conventional spectrometer equipped with a silicon-based CCD array. A Fourier transformation with respect to the time delay between the first two pulses (with wave vectors $\mathbf{k}_1$ and $\mathbf{k}_2$) yields a rephasing 2DIR spectrum. To balance the upconversion bandwidth versus signal intensity, two different $LiNbO_3$ crystals were used: a 0.5-mm crystal was used for the 2DIR experiments and a 4.0-mm crystal for the transient-DVE experiments where less broad-band phase matching is needed. Transient-2DIR spectra were similarly measured by adding a 400 nm pulse chopped at a 50% duty cycle. The first IR pulse was scanned continuously and the heterodyned signal spectrum was detected at the laser repetition rate. The two interferograms (UV pumped and unpumped) were Fourier-transformed separately and the final difference computed in the frequency domain. Transient-DVE signals ($t_1=t_2=0$) were similarly measured by blocking the reference pulse and recording the signal spectrum as a function of the UV-IR delay (τ). This time delay was scanned continuously and DVE spectra were recorded at the laser repetition rate of 1 kHz. The transient DVE intensity (Equation S1) was computed using an integration window of 100 laser shots, corresponding to ~500 fs.

$$\Delta I_{DVE}(t_1 = t_2 = 0, \omega_3, \tau) = \frac{I_{DVE,Pump} - I_{DVE,\mathrm{Pr}obe}}{I_{DVE,\mathrm{Pr}obe}} \qquad \text{(S1)}$$

In the above equation, $I_{DVE,Pump}$ and $I_{DVE,\mathrm{Pr}obe}$ represent the DVE signal intensity with and without the UV pulse respectively. A flow-cell with 2-mm CaF_2 windows and a 100-μM spacer was used to flow the sample solution into the interaction region. To minimize scattering of the UV pulse arising from photoproducts accumulating on the CaF_2 windows, the flow-cell was also scanned continuously during the data acquisition process. In addition to the 400-nm transient-DVE experiments, in ethyl acetate the bleach recovery for the 1958 cm^{-1} peak was measured in n-hexane, using a 400-nm pump as well as a 515-nm pump (10μJ, ~200 fs, $\Delta\lambda$ ~ 80 nm) obtained from the output a non-collinear optical parametric amplifier (NOPA). These experiments in a non-polar solvent were performed so as to be able to directly compare the measured rebinding rate constants with the previously published values obtained from 515nm-pump/400nm-probe transient absorption experiments.[3]All chemicals were purchased from Sigma-Aldrich and were used without further purification. Before collection of the 2DIR spectra, the sample cell was placed in a standard FTIR spectrometer to measure the linear absorption spectrum and to measure the optical

density (OD) at the carbonyl stretching frequencies. To minimize spectral distortions in the 2DIR spectra, it was necessary to keep the optical density below ~0.5 at the frequency of interest.

The dispersed vibrational echo signal is given by the projection of the squared modulus of the 2DIR signal along the detection axis. In other words, it is integrated over the excitation frequency ω_1. Due to the four field interactions (three provided by the laser and the fourth generated by the induced polarization), a diagonal feature appearing at the frequency ω_{0a} in the complex 2DIR spectrum is proportional to $\vec{\mu}_{0a}\vec{\mu}_{0a}\vec{\mu}_{0a}\vec{\mu}_{0a}$, where $\vec{\mu}_{0a}$ is the transition dipole moment between the ground state, 0, and an excited state, *a*. The DVE signal is the ω_1-integrated square modulus of the complex 2DIR signal, and thus the same diagonal feature contributes to the DVE spectrum as a term proportional to $\left|\vec{\mu}_{0a}\vec{\mu}_{0a}\vec{\mu}_{0a}\vec{\mu}_{0a}\right|^2$. By contrast the linear absorption associated with the same transition is proportional to $\vec{\mu}_{0a}\vec{\mu}_{0a}$, thus the higher power dependence of the DVE serves to enhance the sharpness of the spectral features of the spectrum relative to the effectively linear absorption probed by transient absorption. To account for peak broadening or small spectral shifts caused by increased temperatures at early UV-IR time delays, the curves in Figures 2a and 2b are obtained by integrating over the DVE peaks (centered at 1958 and 2013 cm^{-1} respectively) instead of monitoring a single-frequency. This integration is expected to yield amplitudes that independent of temperature (which may induce broadening in the lineshape).

Computational Methods

Electronic-structure computations of the potential energy surface along the Mo-Mo bond and rotation angle of each monomer were carried out using unrestricted Hartree-Fock theory. This method was chosen over density functional theory as it provides a better description of long-range interactions. A mixed basis set using LanL2DZ[4] on the metal centers and a 6-31G(d) basis on the remaining atoms was used. A harmonic vibrational analysis on the equilibrium geometries confirmed that these are stationary points. Starting from the equilibrium geometry in the *trans* conformation, a potential energy surface was obtained by computing single-point energies at seven values along the metal-metal bond, and twelve angles from *trans* (0^o) to *cis* (90^o). Since Hartree-Fock results tend to grossly overestimate energies in comparison with experiment, all the computed energies were scaled by an empirical factor of 0.62. This factor was obtained by comparing the computed to the experimental ΔH of isomerization. Since the reaction coordinate for isomerization at the equilibrium bond distance is likely more complicated than a simple rotation of one of the monomers around the metal-metal bond, the potential energy surface was computed starting at 0.5 $\AA$ up to 2.2 $\AA$ from the equilibrium bond distance. All electronic-structure computations were carried out using the Gaussian 03 program.[5]

Electronic Structure Results

Optimized UHF energies and parameters are shown in Table S.1 below. The raw electronic structure results show an isomerization energy of 5.01 kJ/mol, a factor of 1/0.62 (i.e. 1.6) higher than the experimental value. A high-level density functional theory analysis of all the stable isomers in $[CpMo(CO)_3]_2$ has been recently reported in the literature.[6]

Table S.1. Optimized UHF energies and selected geometry parameters.

UHF Energies			
	Trans	**Gauche**	**Difference**
Energy (a.u.)	-1194.693175	-1194.691233	5.01 kJ/mol
ZPE (a.u)	0.234704	0.234408	
Entropy (J/mol K)	709.19218	713.27577	4.08 J/ mol K
Selected UHF Geometry Parameters			
Mo-Mo Distance (Angstroms)	3.413	3.352	
Mo2-Mo1-C1 Angle (Deg)	132.51	129.214	
C1-Mo1-Mo2-C2 Dihedral (Deg)	180.0	105.72	
C1-O1 Distance (Angstroms)	1.1281	1.16	

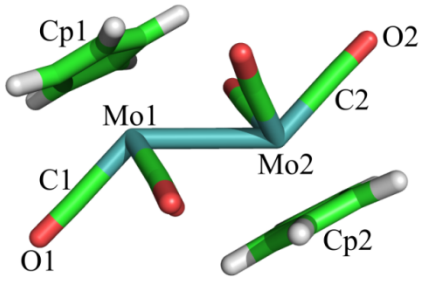

Figure S.2—Optimized geometry of the *trans* isomer showing selected atom labels. Some geometry parameters are shown in Table S.1.

Table S.2. Cartesian coordinates ($\AA$) corresponding to the UHF optimized geometries for the trans and gauche configurations.

	Trans			Gauche		
Atom	x	y	z	x	y	z
Mo	0.0077	-0.0128	-0.2066	-0.6432	0.8876	1.1172
Mo	-0.0087	0.0121	3.2066	2.5351	-0.3310	0.9885
C	1.9503	0.0106	0.4696	-2.1278	2.0856	-0.3151
C	0.8385	-1.3121	-1.5956	-2.5859	0.7415	-0.2607
C	-0.8295	-1.7660	0.4692	-1.6233	-0.0711	-0.8994
C	-1.3645	0.8130	-1.9734	-0.5773	0.7648	-1.3509
C	-2.0707	1.1098	-0.7885	-0.8847	2.0950	-0.9863
C	-1.3160	2.0581	-0.0595	3.5990	-2.4636	0.8846
C	-0.1382	2.3450	-0.7881	2.2327	-2.7467	1.1056
C	-0.1649	1.5797	-1.9731	1.5125	-2.3339	-0.0381
C	-1.9513	-0.0112	2.5305	2.4285	-1.7871	-0.9647
C	0.8285	1.7653	2.5308	3.7205	-1.8677	-0.3998
C	-0.8395	1.3115	4.5956	4.3607	0.4979	1.5152
C	0.1639	-1.5804	4.9732	2.1472	0.0128	2.9920
C	0.1371	-2.3457	3.7881	2.4030	1.4154	-0.0868
C	1.3149	-2.0588	3.0596	-1.8888	1.3475	2.7092
C	2.0697	-1.1106	3.7886	-0.5297	-0.9001	2.1246
C	1.3635	-0.8137	4.9735	0.5428	2.3174	2.0292
O	3.0402	0.0601	0.7543	5.3701	0.9081	1.7815
O	1.2733	-1.9914	-2.3753	1.9862	0.1252	4.1001
O	-1.3323	-2.7343	0.7537	-2.5980	1.6044	3.5394
O	-1.2743	1.9908	5.3754	2.4183	2.3301	-0.7468
O	1.3314	2.7336	2.2464	-0.5827	-1.8984	2.6470
O	-3.0411	-0.0609	2.2457	1.1328	3.1585	2.4885
H	-3.0277	0.7190	-0.5087	2.1943	-1.4255	-1.9457
H	-1.6068	2.5128	0.8645	0.4602	-2.4499	-0.1905
H	0.6183	3.0494	-0.5079	1.8186	-3.2276	1.9681
H	0.5592	1.6180	-2.7621	4.4070	-2.7133	1.5427
H	-1.7030	0.1719	-2.7626	4.6357	-1.5881	-0.8821
H	-0.5603	-1.6186	5.7621	-3.5245	0.4099	0.1362
H	-0.6194	-3.0500	3.5079	-2.6602	2.9477	0.0336
H	1.6058	-2.5135	2.1356	-0.2977	2.9605	-1.2168
H	3.0267	-0.7197	3.5088	0.2814	0.4506	-1.9059
H	1.7020	-0.1727	5.7626	-1.7017	-1.1275	-1.0605

2DIR Peak Assignment

The absorption spectrum in ethyl acetate (Figure S.3) shows three main peaks centered at 1913, 1958, and 2013 cm^{-1}. The two low-frequency peaks have contributions from the *trans* and *gauche* conformations whereas the 2013 cm^{-1} peak is only due the to *gauche* conformation. It has been previously observed that in non-polar solvents, where only the *trans* conformation is favored, that the high frequency peak is not present and the low frequency peaks become narrower. Thus it was predicted that the two isomers would have overlapping transitions near 1913 and 1958 cm^{-1}. This assignment is confirmed by the equilibrium 2DIR spectrum shown in Figure S.3. The spectrum shows cross peaks between all three main diagonal peaks, at zero waiting time, the only possible route to cross peaks is a common ground-state between the transitions, therefore, in addition to the high-frequency transition, the *gauche* isomer has transitions that overlap those of the *trans* isomer. This simple peak assignment is one clear example of the inherent structure-specific spectral information provided by 2DIR spectroscopy.

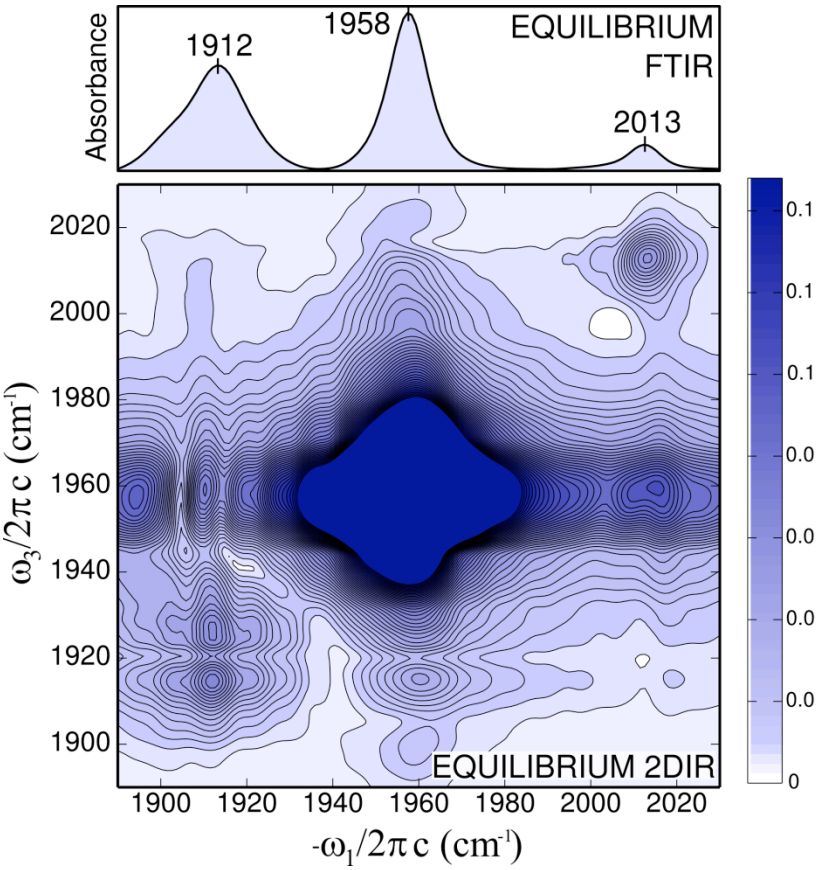

Figure S.3 – (top) Absorption spectrum of $[CpMo(CO)_3]_2$ in ethyl acetate. (bottom) Absolute value rephasing 2DIR spectrum measured with all-parallel polarizations at zero waiting time (i.e. $t_2 = 0$). The spectrum shows cross-peaks between all three main peaks.

Further Discussion of Recombination Reactions in $[CpMo(CO)_3]_2$ and Analogs

The diffusive *trans/gauche* recombination ratios of $[(n\text{-butylCp})Mo(CO)_3]_2$ in various solvents have been measured using microsecond time-resolved absorption spectroscopy.[7] These ratios are observed to be highly dependent on the solvent polarity and viscosity, with viscous non-polar solvents significantly favoring the *trans* configuration (15:1 ratio in n-heptane). The studies also measured the *gauche*-to-*trans* isomerization rate constants and found these to be on the order of $k_{G\rightarrow T} = 1.1\times10^3\ s^{-1}$ at 283 K. Because of the slow exchange kinetics compared to the timescale of our experiments (50 ps), the *gauche* and *trans* populations can be considered static with exchange only occurring via bond cleavage/recombination (i.e. via the photochemical reaction). A separate study has reported that the *gauche* isomer is significantly favored in the diffusion-limited recombination of $[CpMo(CO)_3]_2$.[8] These two results are somewhat conflicting with those of $[(n\text{-butylCp})Mo(CO)_3]_2$ as it is not expected that slightly modifying the Cp ligand would significantly affect these ratios. Therefore a careful study of the nature of the aromatic ligand on the diffusive recombination ratio may lead to a reinterpretation of these experimental results. Although our measurements are on the solvent-caged radical pairs and on a vastly different timescale, they show that the *trans* isomer is greatly favored in polar solvents. Detailed studies on cage escape rates and recombination efficiencies have been reported in the literature.[9-10] These studies were carried out using transient absorption in the visible with a 515-nm pump. The results indicate that the recombination efficiency can vary widely from 10% to 90% and is proportional to $mass^{1/2}radius^{-2}$ for different substituted Cp ligands.

Oelkers and coworkers have measured the solvent-caged radical rebinding rate constants for $[CpMo(CO)_3]_2$ in several solvents using transient absorption spectroscopy with a 515-nm pump and 400-nm probe.[3] The values obtained range from 3.5 ps in pentane to 8.0 ps in 1-propanol. These rebinding rates are significantly faster than the results measured in our 400-nm pump/DVE-probe experiments. In an attempt to understand this difference in rebinding rates we repeated the transient-DVE experiments by monitoring the bleach recovery of the 1958 cm^{-1} parent peak in n-hexane using the 400-nm pump as well as a 515-nm pump to directly compare the results with those of Oelkers *et al.* The measured rebinding curves (shown in Figure S.4 below) exhibit decay times of 19.3±0.6 and 16.5±0.5 ps corresponding to rebinding rate constants of 38.6±1.2 and 33.0±1.0 ps for 400-nm and 515-nm pump respectively, much greater than the 5.6±1 ps measured by Oelkers *et al*. Note that these new experiments were performed on a different date than the one reported in the main text, however the two 400-nm rebinding rates (31.6 ps and 33.0 ps) are within experimental error of each other. In an attempt to understand the difference in rebinding rates measured with electronic and vibrational probes we have also successfully reproduced their experimental transient-absorption results obtaining a value of 4.6±0.5 ps in n-hexane. Although the actual rebinding rate constants are not the central topic of investigation and do not directly determine the main conclusion of this work, this discrepancy certainly war-

rants further investigation. At this point, any explanations that we can imagine of the large rebinding rate disparity are highly speculative. It is also worth noting that the choice of pump wavelength has a measurable but slight, effect on the rebinding rates. This evidence suggests that the two different excited states may lead to different dissociative potentials.

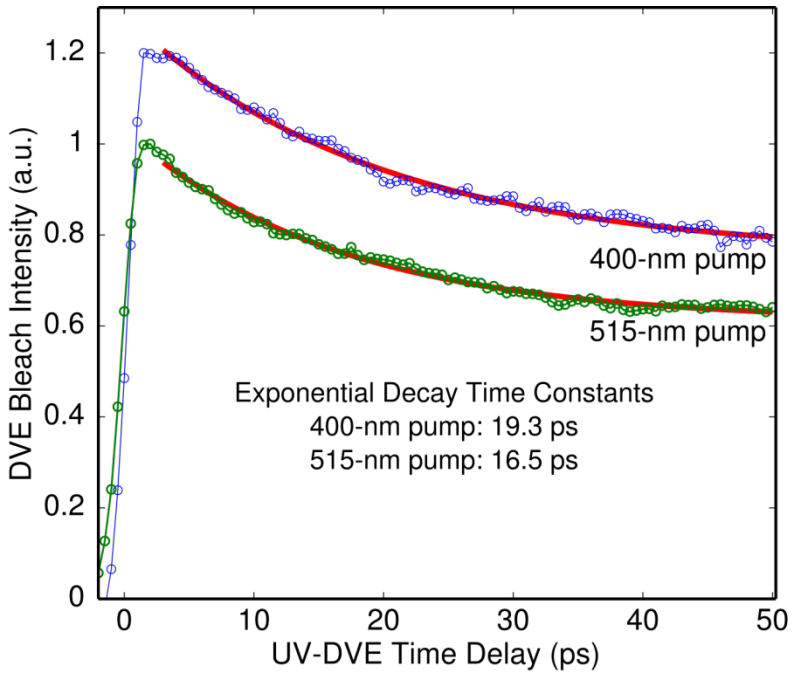

Figure S.4 – Transient DVE bleach recoveries of the 1958 cm^{-1} of $[CpMo(CO)_3]_2$ in n-hexane along with the respective single-exponential fits. The rebinding rates were measured using two different pump wavelengths. The two curves are offset for clarity.

Finally, another important issue that should be discussed in this context is the orientational relaxation of the monomers. The basic question is: How long in time do the monomers retain a memory of their pre-cleavage conformation? The orientational correlation time constants of the monomers inside the solvent cage have been carefully measured in various non-polar solvents by Oelkers and coworkers.[3] These time constants were found to depend linearly on the viscosity of the solvent. The solvent used for our experiments has a viscosity of 0.423 cP at 298 K,[11] so according to their results, one would predict an orientational relaxation time of approximately 6 ps. This measurement, combined with our measured recombination time constant of 31.6 ps, indicates that the radical caged-pairs start out completely randomized in the orientational coordinate before rebinding. In ethyl acetate, we do not observe significant recombination into the *gauche* isomer, an observation which, when combined with the computed PES, suggests that orientational energy landscape "steers" the molecules towards the more stable *trans* conformation.

Further Discussion of the Theoretical Models

The computed PES shows the thermally accessible area at 300K along the Mo-Mo bond rotation coordinate at each point in the Mo-Mo distance coordinate. Since the molecules have a large excess energy after photodissociation with vibrational cooling occurring in the same timescale as the experiment it is unlikely that the molecules are in full thermal equilibrium during the rebinding process. The temperature of the $CpMo(CO)_3$ radicals after photodissociation can be estimated from the initial photon energy, bond energy, and the *ab-initio* heat capacity.[6] This temperature is estimated to be 750K, a significant increase from the equilibrium temperature of 300K. Evidence for rapid vibrational cooling, however, can be found in the absorption linewidths of the photoproduct peaks. In metal carbonyls, excitation of the low-frequency modes of the molecule, due to a temperature increase, causes the high-frequency peaks to broaden due to anharmonic coupling in the vibrational Hamiltonian.[12-13] Measuring the absorption linewidth as a function of UV-IR time delay in $CpMo(CO)_3$ we observe that the linewidths remain narrow even at short delays after photodissociation, which is direct evidence for rapid vibrational cooling. This is not surprising since the photoproduct molecules have a large number of low-frequency modes that can efficiently transfer energy to the solvent by resonantly coupling to the solvent modes. We expect that future modeling of this reaction will include temperature effects as well as properly modeling the excited-state potentials.

References

(1) Nee, M. J.; McCanne, R.; Kubarych, K. J.; Joffre, M. *Optics Letters* **2007**, *32*, 713-715.

(2) Baiz, C.; Nee, M.; McCanne, R.; Kubarych, K. *Opt. Lett.* **2008**, *33*, 2533-2535.

(3) Oelkers, A. B.; Scatena, L. F.; Tyler, D. R. *Journal of Physical Chemistry A* **2007**, *111*, 5353-5360.

(4) Hay, P. J.; Wadt, W. R. *The Journal of Chemical Physics* **1985**, *82*, 270-283.

(5) Frisch, M. J.; Trucks , G. W.; Schlegel , H. B.; Scuseria , G. E.; Robb, M. A.; Cheeseman, J. R.; Montgomery Jr., J. A.; Vreven, T.; Kudin, K. N.; Burant, J. C.; Millam, J. M.; Iyengar, S. S.; Tomasi, J.; Barone, V.; Mennucci, B.; Cossi, M.; Scalmani, G.; N. Rega ; G. A. Petersson ; H. Nakatsuji ; M. Hada ; M. Ehara ; K. Toyota ; R. Fukuda ; J. Hasegawa ; M. Ishida ; T. Nakajima ; Y. Honda ; O. Kitao ; H. Nakai ; M. Klene ; X. Li , J. E.; Knox , H. P.; Hratchian ; Cross , J. B.; Bakken , V.; Adamo , C.; Jaramillo , J.; Gomperts , R.; Stratmann , R. E.; Yazyev , O.; Austin , A. J.; Cammi , R.; Pomelli , C.; Ochterski , J. W.; Ayala , P. Y.; Morokuma , K.; Voth , G. A.; Salvador , P.; Dannenberg , J. J.; Zakrzewski , V. G.; Dapprich , S.; Daniels , A. D.; Strain , M. C.; Farkas , O.; Malick , D. K.; Rabuck , A. D.; Raghavachari , K.; Foresman , J. B.; Ortiz , J. V.; Cui , Q.; Baboul , A. G.; Clifford , S.; Cioslowski , J.; Stefanov , B. B.; Liu , G.; Liashenko , A.; Piskorz , P.; Komaromi , I.; Martin , R. L.; Fox , D. J.; Keith , T.; Al-Laham , M. A.; Peng , C. Y.; Nanayakkara , A.; Challacombe , M.; Gill , P. M. W.; Johnson , B.; Chen , W.; Wong , M. W.; Gonzalez , C.; Pople, J. A.; Gaussian, Inc.: Wallingford CT, 2004.

(6) Zhang, X.; s. Li, Q.; Ge, M.; Xie, Y.; King, R. B.; Schaefer, H. F. *Organometallics* **2009**, *28*, 2818 - 2829.

(7) Linehan, J. C.; Yonker, C. R.; Addleman, R. S.; Autrey, S. T.; Bays, J. T.; Bitterwolf, T. E.; Daschbach, J. L. *Organometallics* **2001**, *20*, 401-407.

(8) Peters, J.; George, M. W.; Turner, J. J. *Organometallics* **1995**, *14*, 1503-1506.

(9) Oelkers, A. B.; Tyler, D. R. *Photochemical & Photobiological Sciences* **2008**, *7*, 1386 - 1390-1386 - 1390.

(10) Oelkers, A. B.; Schutte, E. J.; Tyler, D. R. *Photochemical & Photobiological Sciences* **2008**, *7*, 228-234.
(11) Lide, D. R. *CRC handbook of chemistry and physics: A ready-reference book of chemical and physical data*; CRC press, 2004.
(12) Steinhurst, D. A.; Baronavski, A. P.; Owrutsky, J. C. *Chemical Physics Letters* **2002**, *361*, 513-519.
(13) Baiz, C. R.; McCanne, R.; Nee, M. J.; Kubarych, K. J. *The Journal of Physical Chemistry A* **2009**, *113*, 8907-8916.